Fermilab Library
0 1160 0021826 7

PRINT-92-0590

BUTP-92/50

A determination of the low energy parameters of the 2-d Heisenberg antiferromagnet

U.-J. Wiese[1,+] and H.-P. Ying[1,2]

[1] Institut für Theoretische Physik, Universität Bern, Sidlerstrasse 5, CH-3012 Bern, Switzerland

[2] Zhejiang Institute of Modern Physics, Zhejiang University, Hangzhou 310027, P. R. China

December 3, 1992

Abstract

We perform numerical simulations of the 2-d antiferromagnetic quantum Heisenberg model using an efficient cluster algorithm. Comparing the finite size and finite temperature effects of various quantities with recent results from chiral perturbation theory we are able to determine the low energy parameters of the system very precisely. We find $e_0 = -0.6693(1)J/a^2$ for the ground state energy density, $\mathcal{M}_s = 0.3074(4)/a^2$ for the staggered magnetization, $\hbar c = 1.68(1)Ja$ for the spin wave velocity and $\rho_s = 0.186(4)J$ for the spin stiffness. Our results agree with experimental data for the undoped precursor insulators of high-T_c superconductors.

+supported by the Schweizer Nationalfond

The first high-T_c superconductor to be discovered was $La_{2-x}Ba_xCuO_4$ with $x \approx 0.15$ [1], which has a layered structure with 2-d copper-oxygen planes. The copper ions are located at the sites of a quadratic lattice with lattice spacing $a = 3.79$ Å. The undoped material La_2CuO_4 is an insulator, however, with strong antiferromagnetic interactions within the copper-oxygen planes between electron spins localized at the copper ions. The couplings between different layers are extremely weak. Experimentally one observes long range antiferromagnetic order, i.e. a spontaneous staggered magnetization $\mathcal{M}_s$ arises, which breaks the $O(3)$ spin rotational symmetry down to $O(2)$. The low energy excitations of the system are spinwaves (the so-called magnons) which are the Goldstone bosons of the spontaneously broken $O(3)$ symmetry. The physical situation can be modeled by the 2-d Heisenberg quantum spin system with Hamiltonian

$$H = J \sum_{x,\mu} \vec{S}_x \cdot \vec{S}_{x+\hat{\mu}}, \tag{1}$$

where $\vec{S}_x = \frac{1}{2}\vec{\sigma}_x$ is a spin $\frac{1}{2}$ operator ($\vec{\sigma}_x$ are Pauli matrices) located at the point x of a 2-d quadratic lattice with lattice spacing a. The interaction is between nearest neighbors ($\hat{\mu}$ is the unit vector in μ-direction) and $J > 0$ is the antiferromagnetic exchange coupling. The question arises how well this model describes the physics of the copper-oxygen planes in La_2CuO_4, in particular how it compares quantitatively with experimental results.

Here we concentrate on the calculation of the low energy parameters of the model, which determine the dynamics of the Goldstone bosons. These are the staggered magnetization $\mathcal{M}_s$, the spinwave velocity $\hbar c$ and the spin stiffness ρ_s. Based on symmetry considerations chiral perturbation theory makes very strong predictions for the magnon dynamics, containing the low energy parameters as the only unknown constants. Recently, Hasenfratz and Niedermayer have worked out the chiral perturbation theory for the antiferromagnet in great detail up to two-loop order [2]. Lower order results had been obtained before by Fisher [3] and by Neuberger and Ziman [4]. Here we only quote the results of ref.[2] that are essential for our study. We consider the system at finite temperature T and in a finite spatial volume of size $L \times L$ with periodic boundary conditions, with $l^3 = \hbar c/TL$ such that l is of order 1. For small enough temperatures $T \ll 2\pi\rho_s$ and large enough volumes $\hbar c/L \ll 2\pi\rho_s$ Hasenfratz and Niedermayer obtained the following results: for the internal energy density

$$e(T,L) = e_0 - \frac{T}{3L^2}\left\{1 + l\frac{d}{dl}\beta_0(l) - \frac{\hbar c}{\rho_s L l}\left[\beta_1(l) - l\frac{d}{dl}\beta_1(l)\right] + \ldots\right\}, \tag{2}$$

where e_0 is the ground state energy density; for the staggered susceptibility

$$\chi_s(T,L) = \frac{\mathcal{M}_s^2 L^2}{3T}\left\{1 + 2\frac{\hbar c}{\rho_s L l}\beta_1(l) + \left(\frac{\hbar c}{\rho_s L l}\right)^2\left[\beta_1(l)^2 + 3\beta_2(l)\right] + \ldots\right\}; \tag{3}$$

and for the uniform susceptibility

$$\chi(T,L) = \frac{2\rho_s}{3(\hbar c)^2}\left\{1 + \frac{1}{3}\frac{\hbar c}{\rho_s Ll}\tilde{\beta}_1(l) + \frac{1}{3}\left(\frac{\hbar c}{\rho_s Ll}\right)^2\left[\tilde{\beta}_2(l) - \frac{1}{3}\tilde{\beta}_1(l)^2 - 6\psi(l)\right] + ...\right\}. \tag{4}$$

The functions $\beta_i(l)$, $\tilde{\beta}_i(l)$ and $\psi(l)$ are shape coefficients which depend only on l and which are described in detail in ref.[2]. We will use these results of chiral perturbation theory to determine the unknown low energy parameters e_0, $\mathcal{M}_s$, $\hbar c$ and ρ_s from a fit of $e(T,L)$, $\chi_s(T,L)$ and $\chi(T,L)$ to numerical Monte Carlo data. This method has been used before for classical spin models and for relativistic quantum field theories [5].

First we decompose the Hamiltonian into $H = H_1 + H_2 + H_3 + H_4$ with

$$H_1 = J\sum_{x=(2m,n)} \vec{S}_x\cdot\vec{S}_{x+\hat{1}},\quad H_2 = J\sum_{x=(m,2n)} \vec{S}_x\cdot\vec{S}_{x+\hat{2}},$$
$$H_3 = J\sum_{x=(2m+1,n)} \vec{S}_x\cdot\vec{S}_{x+\hat{1}},\quad H_4 = J\sum_{x=(m,2n+1)} \vec{S}_x\cdot\vec{S}_{x+\hat{2}}, \tag{5}$$

and we use the Suzuki-Trotter formula for the partition function

$$Z = \mathrm{Tr}\exp(-\beta H) = \lim_{N\to\infty}\mathrm{Tr}[\exp(-\epsilon\beta H_1)\exp(-\epsilon\beta H_2)\exp(-\epsilon\beta H_3)\exp(-\epsilon\beta H_4)]^N, \tag{6}$$

where $\beta = 1/T$ is the inverse temperature and $\epsilon = 1/N$ determines the lattice spacing in the euclidean time direction. By inserting complete sets of eigenstates $|1\rangle$ and $|-1\rangle$ of σ_x^3 between the factors $\exp(-\epsilon\beta H_i)$ we map the 2-d quantum spin system to a 3-d induced classical system of Ising-like variables $s(x,t) = \pm 1$ (t labels the euclidean time slice)

$$Z = \prod_{x,t}\sum_{s(x,t)=\pm 1}\exp(-S) \tag{7}$$

with an action

$$\begin{aligned} S = &\sum_{x=(2m,n),t=4p} S[s(x,t),s(x+\hat{1},t),s(x,t+1),s(x+\hat{1},t+1)] \\ &+ \sum_{x=(m,2n),t=4p+1} S[s(x,t),s(x+\hat{2},t),s(x,t+1),s(x+\hat{2},t+1)] \\ &+ \sum_{x=(2m+1,n),t=4p+2} S[s(x,t),s(x+\hat{1},t),s(x,t+1),s(x+\hat{1},t+1)] \\ &+ \sum_{x=(m,2n+1),t=4p+3} S[s(x,t),s(x+\hat{2},t),s(x,t+1),s(x+\hat{2},t+1)]. \end{aligned} \tag{8}$$

The classical spins interact with each other via four-spin couplings $S[s(x,t),s(x+\hat{\mu},t),s(x,t+1),s(x+\hat{\mu},t+1)]$ associated with time-like plaquettes. Up to a trivial additive constant one has $S[1,1,1,1] = S[-1,-1,-1,-1] = 0$, $S[1,-1,1,-1] = S[-1,1,-1,1] = -\log[\frac{1}{2}(\exp(\epsilon\beta J)+1)]$ and $S[1,-1,-1,1] = S[-1,1,1,-1] = -\log[\frac{1}{2}(\exp(\epsilon\beta J)-1)]$. All other action values are infinite. This causes problems in numerical simulations because many spin configurations are forbidden and the updating must respect several constraints. In a previous paper we have introduced blockspins [6] to resolve the constraints. For the 1-d antiferromagnetic spin chain the blockspin model is not frustrated and the use of a blockspin cluster algorithm eliminates critical slowing down. In two dimensions, however, frustration causes severe problems. Recently, Evertz, Lana and Marcu [7] have developed loop cluster algorithms for vertex models, which can also be applied to quantum spin systems. The algorithm constructs closed loops of spins and flips them simultaneously. The loop cluster algorithm does not suffer from frustration but it may suffer from so-called freezing. Freezing occurs when a loop branches out many times and fills a large fraction of the whole volume. We find that freezing does not arise for the Heisenberg antiferromagnet. This is essential for the success of our numerical study.

The algorithm constructs loops by first selecting a starting point (x,t) at random. The spin $s(x,t)$ participates in two plaquette interactions, one at euclidean times before and one at euclidean times after t. When $s(x,t) = 1$ we consider the plaquette interaction at the later time, and for $s(x,t) = -1$ we consider the interaction at the earlier time. The corresponding plaquette configuration is characterized by the spin orientations at the four corners. One of the corners will be the next point on the loop. For configurations $C_1 = [1,1,1,1]$ or $[-1,-1,-1,-1]$ the next point is the time-like nearest neighbor of (x,t) on the plaquette. For configurations $C_2 = [1,-1,1,-1]$ or $[-1,1,-1,1]$ the next point on the loop is with probability $p = 2/(\exp(\epsilon\beta J)+1)$ the time-like nearest neighbor, and with probability $1-p$ the space-like nearest neighbor of (x,t). Finally, for configurations $C_3 = [1,-1,-1,1]$ or $[-1,1,1,-1]$ the next point on the loop is the space-like nearest neighbor of (x,t). Once the next point on the loop is determined the process is repeated until the loop closes. Then all spins on the loop are flipped simultaneously. The algorithm obeys detailed balance, $p(C_i)w(C_i\to C_j) = p(C_j)w(C_j\to C_i)$, where $p(C_1) = 1$, $p(C_2) = \frac{1}{2}(\exp(\epsilon\beta J)+1)$, $p(C_3) = \frac{1}{2}(\exp(\epsilon\beta J)-1)$ and $w(C_i\to C_j)$ is the transition probability to go from a plaquette configuration C_i to C_j. Indeed one has

$$p(C_1)w(C_1\to C_2) = 1 = \frac{1}{p}p = p(C_2)w(C_2\to C_1),$$
$$p(C_2)w(C_2\to C_3) = \frac{1}{p}(1-p) = \frac{1}{2}(\exp(\epsilon\beta J)-1) = p(C_3)w(C_3\to C_2). \tag{9}$$

In our construction a loop cannot branch out and hence freezing does not arise. Cluster algorithms offer the possibility to use improved estimators which reduce the variance of different observables. For example, the uniform susceptibility can be expressed as $\chi a^2 J = \frac{\beta J}{4N}\langle M_C^2/|C|\rangle$, where $4N$ is the number of points in the euclidean time direction, $|C| = \sum_{(x,t)\in C} 1$ is the size of the loop C and $M_C = \frac{1}{2}\sum_{(x,t)\in C} s(x,t)$ is the loop magnetization. It is interesting to note that clusters with nonzero magnetization must wrap around the lattice in the euclidean time direction. Small clusters which do not wrap around the lattice have $M_C = 0$. Similarly, one can define im-

Table 1: Numerical data for e, χ_s and χ.

βJ	L/a	$4N$	ea^2/J	$\chi_s a^2 J$	$\chi a^2 J$
5	6	256	-0.678(1)	9.67(3)	0.0482(3)
5	8	256	-0.673(1)	16.08(5)	0.0514(3)
5	10	256	-0.672(1)	23.73(7)	0.0527(3)
5	12	256	-0.671(1)	32.3(1)	0.0530(3)
5	14	256	-0.671(1)	41.7(1)	0.0519(3)
5	16	256	-0.669(1)	52.6(2)	0.0531(3)
5	18	256	-0.672(1)	64.3(2)	0.0528(3)
5	20	256	-0.670(1)	76.3(3)	0.0535(3)
10	6	512	-0.679(1)	14.64(5)	0.0268(3)
10	8	512	-0.675(1)	27.5(1)	0.0406(3)
10	10	512	-0.673(1)	42.9(2)	0.0442(3)
10	12	512	-0.673(1)	60.6(2)	0.0460(3)
10	14	512	-0.670(1)	81.2(3)	0.0469(3)
10	16	512	-0.673(1)	103.1(4)	0.0476(3)
10	18	512	-0.672(1)	129.0(4)	0.0480(3)
10	20	512	-0.671(1)	156.2(5)	0.0477(3)
15	6	768	-0.681(1)	16.71(6)	0.0111(3)
15	8	768	-0.675(1)	34.8(1)	0.0287(3)
15	10	768	-0.674(1)	57.9(2)	0.0385(3)
15	12	768	-0.674(1)	83.8(3)	0.0420(3)
15	14	768	-0.672(1)	113.6(4)	0.0439(3)
15	16	768	-0.671(1)	148.0(5)	0.0451(3)
15	18	768	-0.670(1)	187.0(6)	0.0457(3)
15	20	768	-0.671(1)	227.6(8)	0.0457(3)

proved estimators for the staggered susceptibility χ_s and for the internal energy density e.

Some results of our numerical simulations are collected in table 1. We have performed measurements for three inverse temperatures $\beta J = 5, 10, 15$ and for different spatial sizes $L/a = 6, 8, ..., 20$. We have always performed 10000 loop updates for equilibration followed by 100000 measurements using the improved estimators. The autocorrelation times of the loop cluster algorithm are at most a few sweeps, and we see no indication of critical slowing down. With standard local algorithms it would be impossible to reach temperatures as low as the ones we use here, because of severe problems with slowing down. In table 1 the lattice spacing has been fixed to $\epsilon\beta J = \frac{5}{64}$. We have also performed runs on coarser lattices with $\epsilon\beta J = \frac{5}{32}$ and $\frac{5}{48}$. This allows us to extrapolate our data to the euclidean time continuum limit $\epsilon \to 0$. After the extrapolation we fit the results to the above expressions from chiral

perturbation theory. The data for e, χ_s and χ are all fitted simultaneously. Our best fit with $\chi^2/\text{dof} = 1.4$ is shown in fig 1. The finite size and finite temperature effects of the internal energy density depicted in fig.1a are very small (of the order of our statistical errors), while the effects on the susceptibilities are much larger. For low temperature and small volume some data have been excluded from the fit because for them l is not of order 1. The fit gives the following values for the low energy parameters

$$e_0 = -0.6693(1)J/a^2, \ \mathcal{M}_s = 0.3074(4)/a^2, \ \hbar c = 1.68(1)Ja, \ \rho_s = 0.186(4)J. \quad (10)$$

To our knowledge this is the most accurate determination of these zero temperature and infinite volume properties from a simulation of the partition function at finite temperature and finite volume. The result for the ground state energy density agrees with different zero temperature Monte Carlo calculations [8] which yield $e_0 = -0.6692(1)J/a^2$. Our results are consistent with an analytic expansions around the Ising limit [9] which gives $e = 0.6693(1)J/a^2$ and $\mathcal{M}_s = 0.307(1)/a^2$, but not consistent with a recent large scale numerical study using a standard local algorithm [10] which obtained $\rho_s = 0.199(2)J$. Finally, we compare our results with experimental data. Using inelastic neutron scattering the spin wave velocity $\hbar c = 0.85(3)$eVÅ has been measured [11], while an analysis of Raman scattering data [12] yields $J = 0.128(6)$eV $= 1480(70)$K. Using this together with $a = 3.79$Å the experiments on La_2CuO_4 obtain $\hbar c = 1.75(9)Ja$. This is consistent with our result for the Heisenberg antiferromagnet. Using the experimental values for the spinwave velocity and for the lattice spacing we obtain an independent estimate of the exchange coupling in La_2CuO_4

$$J = 0.133(5)\text{eV} = 1540(60)\text{K}. \quad (11)$$

The agreement between our numerical results and the predictions of chiral perturbation theory confirms that the Heisenberg model has long range antiferromagnetic order, and that its low energy dynamics is dominated by magnons. A precise determination of the low energy parameters that determine the magnon physics was possible only because the loop cluster algorithm is very efficient also at low temperatures. Recently, a loop cluster algorithm has been constructed for lattice fermion systems [13]. This raises hopes that numerical investigations of similar accuracy become feasible for the Hubbard model, and hence for high-T_c superconductors like $La_{2-x}Ba_xCuO_4$.

We are indebted to P. Hasenfratz and F. Niedermayer for making their results available to us prior to publication. We also like to thank them for many interesting discussions about quantum antiferromagnets.

References

[1] J. G. Bednorz and K. A. Müller, Z. Phys. B64 (1986) 189.

[2] P. Hasenfratz and F. Niedermayer, Bern preprint 1992, BUTP-92/46.

[3] D. S. Fisher, Phys. Rev. B39 (1989) 11783.

[4] H. Neuberger and T. Zimann, Phys. Rev. B39 (1989) 2608.

[5] A. Hasenfratz, K. Jansen, J. Jersák, C. B. Lang, H. Leutwyler and T. Neuhaus, Z. Phys. C46 (1989) 257;
I. Dimitrović, P. Hasenfratz, J. Nager and F. Niedermayer, Nucl. Phys. B350 (1991) 893.

[6] U.-J. Wiese and H.-P. Ying, Phys. Lett. A168 (1992) 143.

[7] H. G. Evertz and M. Marcu, talk presented at the 1992 Symposium on Lattice Field Theory, Amsterdam, 15-19 September 1992, Tallahassee preprint (1992), FSU-SCRI-92-165;
H. G. Evertz, G. Lana and M. Marcu, Tallahassee preprint (1992), FSU-SCRI-92-164.

[8] T. Barnes, Int. J. Mod. Phys. C2 (1991) 659.

[9] W. Zheng, J. Oitmaa and C. J. Hamer, Phys. Rev. B43 (1991) 8321.

[10] M. S. Makivić and H.-Q. Ding, Phys. Rev. B43 (1991) 3562.

[11] G. Aeppli, S. M. Hayden, H. A. Mook, Z. Fisk, S.-W. Cheong, D. Rytz, J. Remeika, G. P. Espinosa and A. S. Cooper, Phys. Rev. Lett. 62 (1989) 2052.

[12] R. R. P. Singh et. al., Phys. Rev. Lett. 62 (1989) 2736.

[13] U.-J. Wiese, Bern preprint 1992, BUTP-92/45.

Figure Caption

Fig.1: The fit of the Monte-Carlo data for the internal energy ea^2/J (a), the staggered susceptibility $\chi_s a^4 J/L^2$ (b), and the uniform susceptibility $\chi a^2 J$ (c). The dots, squares and triangles are the Monte-Carlo data for $\beta J = 5$, 10 and 15 respectively. The corresponding fit functions are represented by the solid, dashed and dotted curves.

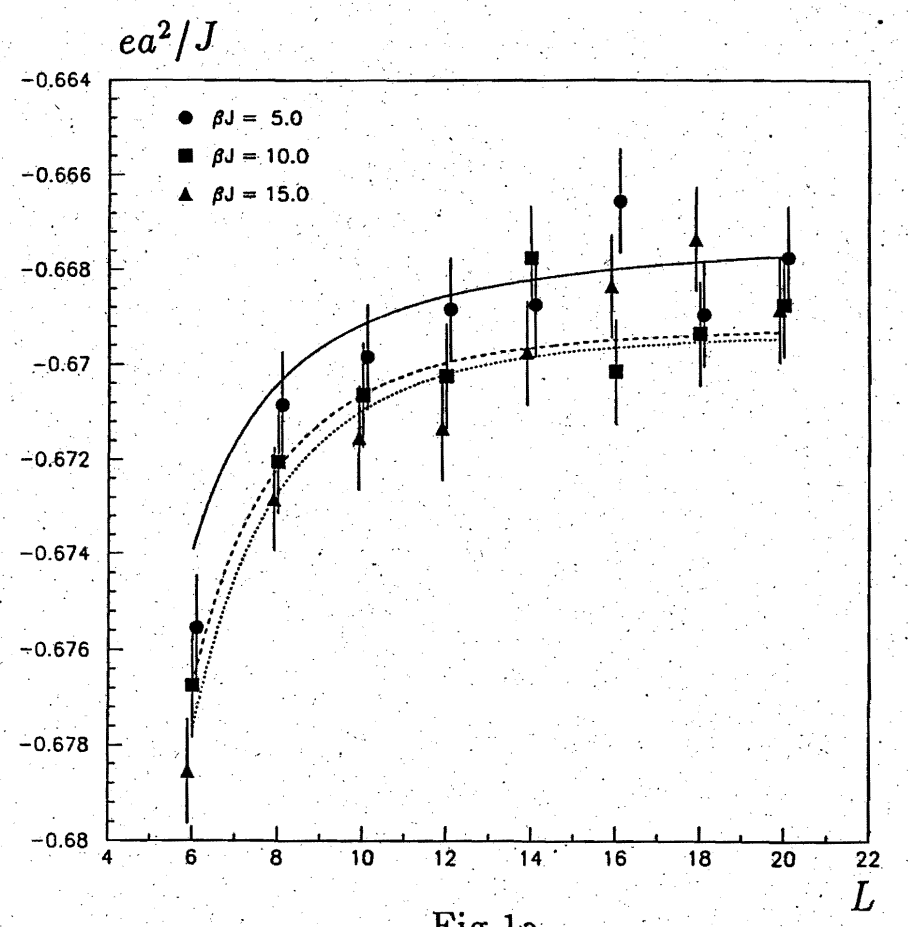

Fig.1a

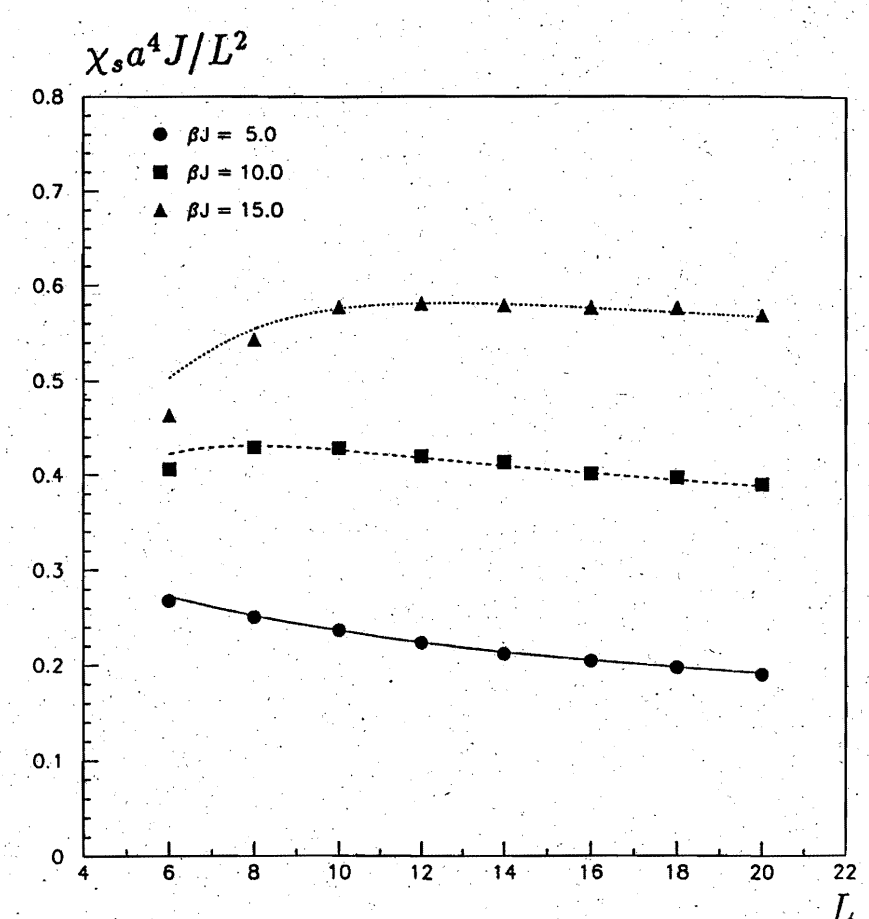
$\chi_s a^4 J/L^2$
βJ = 5.0
βJ = 10.0
βJ = 15.0
0.8
0.7
0.6
0.5
0.4
0.3
0.2
0.1
0
4
6
8
10
12
14
16
18
20
22
L

Fig.1b

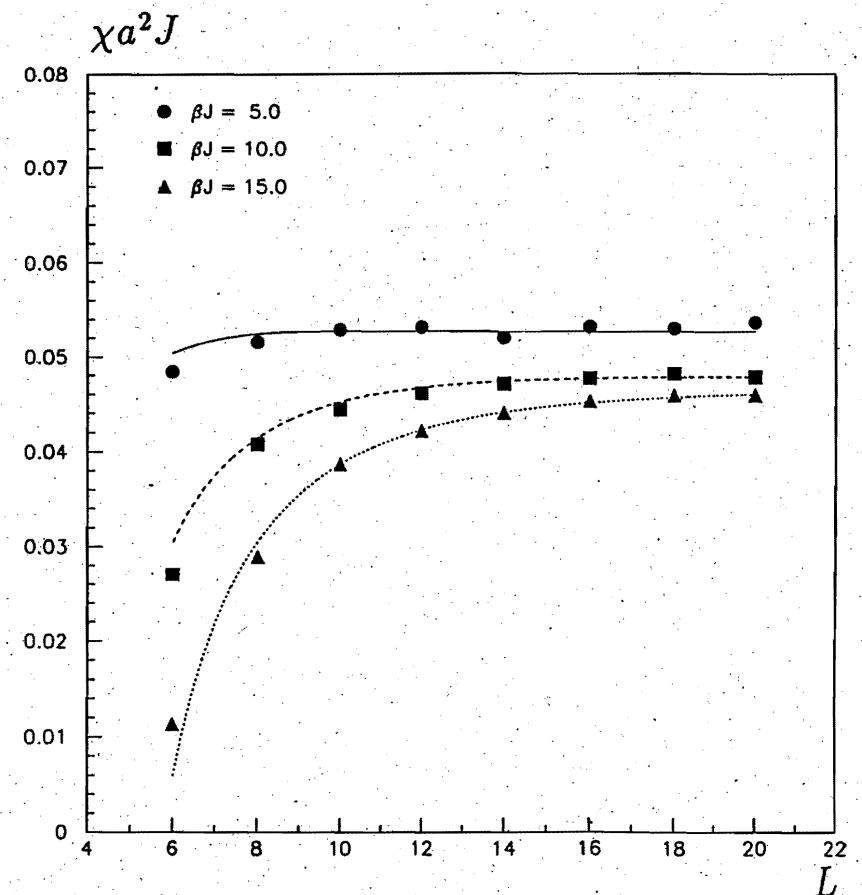
$\chi a^2 J$
βJ = 5.0
βJ = 10.0
βJ = 15.0
0.08
0.07
0.06
0.05
0.04
0.03
0.02
0.01
0
4
6
8
10
12
14
16
18
20
22
L

Fig.1c